Electrochemical and theoretical investigations of the reduction of $[Fe_2(CO)_5L\{\mu\text{-}SCH_2XCH_2S\}]$ complexes related to [FeFe] hydrogenase†

Jean-François Capon,[a] Salah Ezzaher,[a] Frédéric Gloaguen,[a] François Y. Pétillon,[a] Philippe Schollhammer,[a] Jean Talarmin,*[a] Thomas J. Davin,[b] John E. McGrady*[b] and Kenneth W. Muir[b]

Received (in Montpellier, France) 19th June 2007, Accepted 18th July 2007
First published as an Advance Article on the web 17th August 2007
DOI: 10.1039/b709273c

The complexes $[Fe_2(CO)_6\{\mu\text{-}SCH_2N(R)CH_2S\}]$ (R = $CH_2CH_2OCH_3$, **1a**; R = ^{i}Pr, **1b**) and $[Fe_2(CO)_6(\mu\text{-pdt})]$ **2** (pdt = $S(CH_2)_3S$) are structural analogues of the $[2Fe]_H$ subsite of [FeFe]H_2ases. Electrochemical investigation of **1** and **2** in MeCN–$[NBu_4][PF_6]$ under Ar and under CO has demonstrated that the reduction can be resolved into two one-electron transfer steps by using fast scan cyclic voltammetry. At slow scan rates the reduction of **1** tends towards a two-electron process owing to the fast disproportionation of the anion, while the two-electron reduction of **2** is clearly favoured in the presence of CO. Substitution of a CO ligand in **2** by a N-heterocyclic carbene results in the destabilisation of the anion. Thus, in MeCN–, thf- or CH_2Cl_2–$[NBu_4][PF_6]$, the electrochemical reduction of $Fe_2(CO)_5L_{NHC}(\mu\text{-pdt})]$ **3** (L_{NHC} = 1,3-bis(methyl)-imidazol-2-ylidene, **3a**; 1,3-bis(2,4,6-trimethylphenyl)-imidazol-2-ylidene, **3b**) occurs in a single-step, two-electron process at moderate scan rates; under appropriate conditions this process can be separated into two one-electron steps. Density Functional Theory calculations successfully rationalize the effects of the S-to-S linkage on the electrochemistry of the complexes.

1. Introduction

The structural characterization of the functional centre of iron-only hydrogenase,[1] the H-cluster (Scheme 1), has led to a renewed interest in diiron dithiolate complexes of general formula $[Fe_2(CO)_{6-n}(L)_n(\mu\text{-}SR)_2]$[2] because of their resemblance to the organometallic [2Fe] sub-site of the H-cluster that catalyses the $2H^+ + 2e \leftrightarrow H_2$ reaction.

Most of the recently published work concerns {2Fe2S} or {2Fe3S} species that are either all-CO or substituted derivatives with cyanide, phosphine, isocyanide, or N-heterocyclic carbene ligands (NHC); they may also differ in the nature of the bridging atoms (S or P) and the link between them.[2–15] Electrochemical studies have focused on the reduction of the $[Fe_2(CO)_{6-n}(L)_n(\mu\text{-dithiolate})]$ complexes in acidic media. Little, however, is known at this stage about their intrinsic electrochemical properties,[4a,6,7a,15] but the nature of the S-to-S link seems to play a key role in controlling the electron transfer processes. For the all-CO complexes, the μ-sdt derivative (sdt = sulfurdithiolate, SCH_2SCH_2S) reduces through the transfer of two electrons (*i.e.* two reversible one-electron steps with $E_2^\circ - E_1^\circ > 0$)[15] while conflicting results have appeared concerning the reduction of the μ-pdt analogue (pdt = propanedithiolate, $S(CH_2)_3S$) which has been assigned as either a one-electron (Fe^I–$Fe^I \rightarrow Fe^I$–Fe^0)[3a,16] or a two-electron process.[17,18] Recent reports indicate that one electron is involved on the short cyclic voltammetric timescale while bulk electrolysis under CO consumes two electrons per molecule.[4a,6b] Similar ambiguity surrounds the electrochemistry of the closely related complex $[Fe_2(CO)_6(\mu\text{-}SCH_2C_6H_4CH_2S)]$, which may involve either one[3a] or two electrons.[7a] The nature of the dithiolate bridge also seems to affect the reversibility of the electrode processes: while the reduction of $[Fe_2(CO)_6(\mu\text{-sdt})]$ is reversible[15] and that of $[Fe_2(CO)_6(\mu\text{-pdt})]$ partially reversible,[3a,4a,18] the one-electron reduction of $[Fe_2(CO)_6(\mu\text{-adt})]$ (adt = azadithiolate, $SCH_2N(R)CH_2S$; R = C_6H_4Br,[8a] $C_6H_4NH_2$ [8b]) is apparently irreversible.

In addition to the intrinsic interest in resolving these questions, deeper understanding of the effects of specific changes in the coordination sphere of the metal centres on the electrochemistry of dinuclear thiolate-bridged complexes would facilitate the design of more efficient catalysts. Here we focus

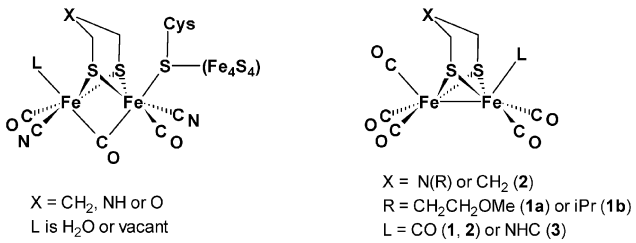

Scheme 1 Schematic representations of the H-cluster of [FeFe] hydrogenases (left) and of the model complexes **1–3** (right).

[a] *UMR CNRS 6521 « Chimie, Electrochimie Moléculaires et Chimie Analytique », UFR Sciences et Techniques, Université de Bretagne Occidentale, CS 93837, 29238 Brest-Cedex 3, France. E-mail: jean.talarmin@univ-brest.fr*
[b] *WestCHEM, Department of Chemistry, University of Glasgow, Glasgow, UK G12 8QQ*

† Electronic supplementary information (ESI) available: Cyclic voltammograms (Fig. S1, S3–S6), scan rate dependence of the current function for **2** (Fig. S2), average lengths and angles (Table S1) and cartesian coordinates and total energies (Table S2) and NR conformations (Fig. S7). See DOI: 10.1039/b709273c

on the primary reduction of $[Fe_2(CO)_{6-n}(L)_n(\mu\text{-SRS})]$ complexes under either argon or CO in an attempt to assess the effects of different constituents on the mechanism of electrochemical reduction. To this end we compare the electrochemistry of $[Fe_2(CO)_6\{\mu\text{-}SCH_2N(R)CH_2S\}]$ (R = $CH_2CH_2OCH_3$, **1a**; R = ^{i}Pr , **1b**) with that of $[Fe_2(CO)_6(\mu\text{-pdt})]$ **2** (Scheme 1) under the same experimental conditions to examine the effects of the S-to-S linkage. The CH_2CH_2OMe arm in **1a** has been designed to mimic the presence of solvent, which may bind to the metal centre at various stages in the electrochemical cycle, thereby protecting any vacant coordination site generated by cleavage of Fe–Fe or Fe–CO bonds. We also reinvestigate the reduction of $[Fe_2(CO)_5(L_{NHC})(\mu\text{-pdt})]$ where L_{NHC} is the N-heterocyclic carbene ligand 1,3-bis(methyl)-imidazol-2-ylidene, **3a**, which we previously assigned as a one-electron process[7b] in contrast to the report on the two-electron reduction of the analogue with L_{NHC} = 1,3-bis(2,4,6-trimethylphenyl)-imidazol-2-ylidene, **3b**.[3f] Comparison of the reduction mechanisms of **2** and **3** provides important information regarding the effects of substituting a CO by an electron-releasing NHC ligand. In all three systems, **1–3**, we show that the electrochemical reduction can be split into two separate one-electron steps under appropriate cyclic voltammetric conditions.

Density functional theory has proved very useful in exploring the electronic structure of hydrogenase and its mimics, and also the intimate mechanism of hydrogen formation.[3–6,19–26] We therefore also report a complementary computational study which explores possible candidates for the various redox events observed in the cyclic voltammograms.

2. Results and discussion

2.1 Synthesis of $[Fe_2(CO)_6\{\mu\text{-}SCH_2N(R)CH_2S\}]$ (R = $CH_2CH_2OCH_3$, 1a; R = ^{i}Pr, 1b) and X-ray crystal structure of 1a

Complexes **1a** and **1b** were obtained by treatment of $[Fe_2(CO)_6(\mu\text{-S})_2]^{2-}$ with *N*,*N*-di(chloromethyl)-2-methoxyethylamine or *N*,*N*-di(chloromethyl)-2-isopropylamine, respectively, following a known procedure[5a,c] (Experimental). We note that the synthesis of a close analogue of **1a** has appeared during the course of our work.[9b] The formulation of **1a** as a bis(μ-thiolato) complex was confirmed by X-ray analysis of a single crystal obtained from hexane–dichloromethane solution. This reveals, as expected, a distorted $S_2(CO)_3$ square-pyramid at each 18-electron iron centre (Fig. 1) and the well-established butterfly structure found in other $[Fe_2(CO)_6\{\mu\text{-}SCH_2N(R)CH_2S\}]$ diiron complexes. Distances and angles in **1a** are unexceptional: for example, the Fe–Fe and mean Fe–S and S–C distances of 2.513(1), 2.249(2) and 1.832(3) Å are barely distinguishable from the corresponding mean values of 2.507, 2.256 and 1.847 Å for all 18 structurally characterised $[Fe_2(CO)_6\{\mu\text{-}SCH_2N(R)CH_2S\}]$ molecules (see Table S1†).[5a,c,d,8a–c,e–g,9a,b,12b,27] The single Fe–Fe bond in **1a** is bridged by both sulfur atoms of the azapropanedithiol ligand, thereby forming boat and chair FeSCNCS rings. Here it is the Fe2–S1–C7–N1–C8–S2 ring which adopts a chair conformation and the methoxyethyl substituent on N1 is in an equatorial position. However, the

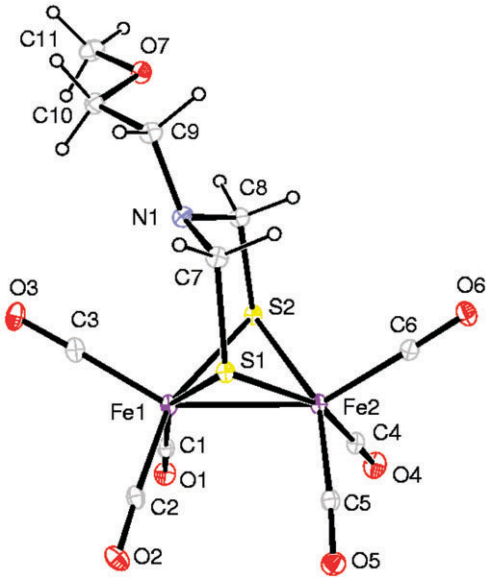

Fig. 1 A view of a molecule of **1a** showing 20% ellipsoids. Selected distances and angles (Å & °): Fe–S 2.245(1)–2.256(1), C7–N1 1.443(2), C8–N1 1.446(2), C9–N1 1.478(2), C7–N1–C8 112.1(2), C7–N1–C9 111.8(1), C8–N1–C9 112.6(1), S1–C7–N1–C9 161.3(1), S2–C8–N1–C9 −161.4(1), Fe2–S1–C7–N1 68.1(1), Fe2–S2–C8–N1 −67.8(1).

N(R) substituent is axial in the closely analogous R = CH_2CH_2OH species.[9b] The N-substituents in $[Fe_2(CO)_6\{\mu\text{-}SCH_2N(R)CH_2S\}]$ complexes show in general almost equal preference for axial and equatorial positions: axial conformations typically have S–CH_2–N–R torsion angles of 83–101° and near trigonal planar coordination at N whereas equatorial conformations are characterised by S–C–N–R torsion angles of 157–168° and more obviously pyramidal nitrogen coordinations (**1a** being typical, see Fig. S7†). DFT calculations suggest that the axial conformer is prefered when R = H but is less stable than the equatorial conformer when R = Me.[9c] The equatorial position of the R = CH_2CH_2OMe substituent in **1a** implies that the nitrogen lone pair points towards Fe1 and the Fe1···N1 and C3···N1 distances [3.279(1) & 3.015(2) Å] seem short. In contrast, the axial H atoms on C7 and C8 do not interact significantly with Fe2 or the C6–O6 carbonyl ligand. The slight (0.03 Å) lengthening of the exocyclic N–CH_2 bond in **1a** relative to the endocyclic N–CH_2 bonds is found in all similar $[Fe_2(CO)_6\{\mu\text{-}SCH_2N(R)CH_2S\}]$ complexes.

We have previously noted that the CH_2CH_2OMe arm was introduced into **1a** in order to mimic possible coordination of a water molecule to a vacant site created by Fe–Fe bond

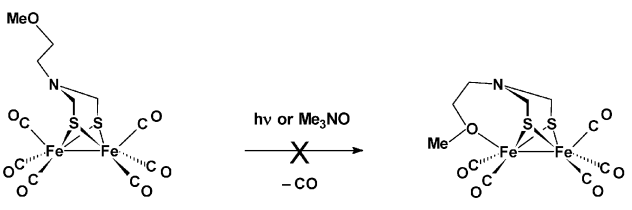

Scheme 2

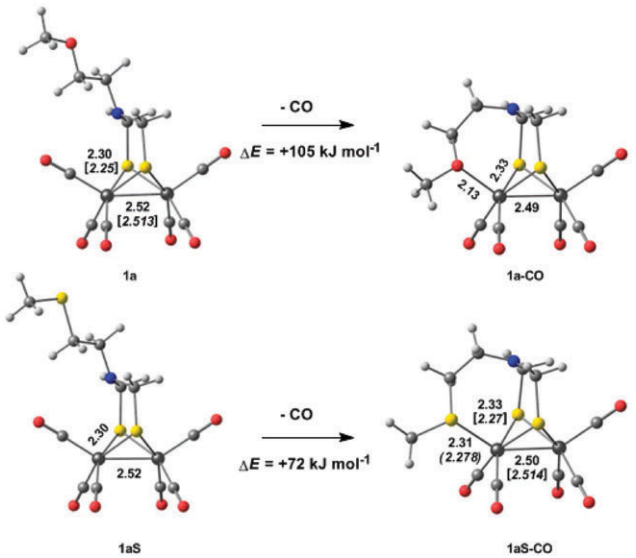

Fig. 2 Optimised structures of **1a** and its decarbonylated derivative, **1a–CO**, along with the thioether analogues (**1S** and **1S–CO**). Crystallographic data for **1a** and **1aS–CO** are given in italics.

cleavage or CO dissociation (Scheme 2). Rauchfuss has described a similar process in the analogue of **1a** with a thioether arm, where CO abstraction using Me_3NO leads to the coordination of the sulphur donor.[5a] However, all attempts to force the coordination of the pendant ether group in **1a** by treatment with Me_3NO, heating in refluxing toluene or irradiation have proved unsuccessful, yielding only a black insoluble material.

The apparent failure of this reaction in the case of **1a** caused us to question whether the weaker electron donating ability of the OMe group relative to SMe was sufficient to prevent coordination to the metal centre. To explore this issue, we used density function theory to probe the energetics of the reaction shown in Scheme 2 for **1a** and its thioether analogue, **1aS**. Structural parameters and total energies of the different species are summarised in Fig. 2. The optimised Fe–Fe bond length in **1a** is in excellent agreement with experiment (2.52 Å *vs.* 2.513(1) Å), as is that in the decarbonylated thioether analogue **1aS–CO** (2.50 Å *vs.* 2.514 Å) which has been crystallographically characterised by Rauchfuss and co-workers.[5a] The loss of CO is endothermic in both cases, but when the subsequent reaction of CO with Me_3NO to form Me_3N + CO_2 ($\Delta E = -320$ kJ mol^{-1} at the same level of theory) is taken into account, it is clear that the relatively minor changes on going from SMe to OMe should not prevent coordination of the pendant arm, at least on thermodynamic grounds. The failure to form the decarbonylated species **1a–CO** shown in Scheme 2 must therefore reflect either an alternative decomposition route or a substantial kinetic barrier to CO loss.

2.2 Electrochemical reduction of the diiron hexacarbonyl dithiolate-bridged complexes $[Fe_2(CO)_6\{\mu\text{-}SCH_2N(R)CH_2S\}]$ (R = $CH_2CH_2OCH_3$, 1a; R = ^{i}Pr, 1b) and $[Fe_2(CO)_6(\mu\text{-pdt})]$, 2 under Ar or CO

2.2.1 Cyclic voltammetry studies. The electrochemical reduction of **1** was investigated by cyclic voltammetry (CV) in MeCN–$[NBu_4][PF_6]$ under Ar and under CO. Complex **2** was examined under the same conditions for comparison. Reproducible CV curves were obtained provided the vitreous carbon disc was polished on a wet felt tissue with alumina. In the present study, this operation was repeated before each individual CV scan.

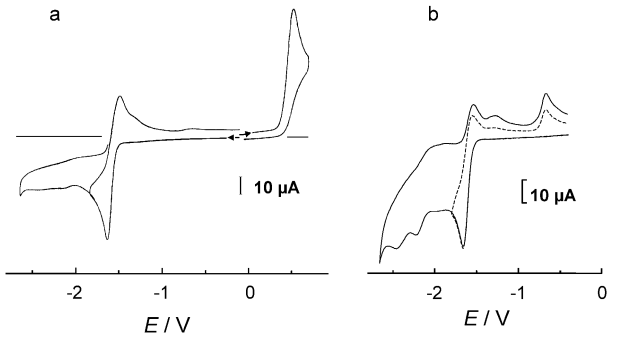

Fig. 3 Cyclic voltammetry of (a) $[Fe_2(CO)_6\{\mu\text{-}SCH_2N(CH_2CH_2OMe)CH_2S\}]$ **1a** (0.83 mM) and (b) $[Fe_2(CO)_6\{\mu\text{-}S(CH_2)_3S\}]$ **2** (*ca.* 1.5 mM) under Ar in MeCN–$[NBu_4][PF_6]$ (v = 0.2 V s^{-1}; vitreous carbon electrode; potentials are in V *vs.* Fc^+/Fc).

The CV of **1a** (Fig. 3a, Table 1) shows a partially reversible reduction that is also present at similar potentials in **1b** (Fig. S1†). The partial reversibility of this reduction stands in sharp contrast to recent reports of the irreversible reduction of several analogues of **1**.[8a,b,9b] The reduction of **2** was also found to be partially reversible under Ar at moderate scan rate (Fig. 3b): the peak current ratio $[(i_p^a/i_p^c)^{red1}]$[28,29] increases from 0.5 to 0.7 when the scan rate is increased from 0.1 V s^{-1} to 1 V s^{-1}, in agreement with previous studies of this complex.[18] A comparison of the CVs in Fig. 3 and S1† clearly shows that the reduction of the complexes with an azadithiolate bridge (**1a**, **1b**) is chemically more reversible than that of the propanedithiolate analogue. In all cases the occurrence of follow-up reactions is indicated by the presence of several product peaks at potentials more negative than that for the primary reduction of the complexes and on the return scan. A detailed investigation of the products formed upon reduction of **2** has been published.[4a]

The reduction of **1** and **2** was examined by cyclic voltammetry at scan rates up to 60 V s^{-1} in order to separate the primary electron transfer steps from the ensuing chemistry. The current function $[(i_p^c)^{red1}/v^{1/2}]$ associated with the first reduction of the complexes over the range 0.02 V s^{-1} $\leq v \leq$ 60 V s^{-1} deviates markedly from linearity at slow scan rates (Fig. 4 and Fig. S2†), which demonstrates that the electrode process tends towards a two-electron transfer on the longer time scale. Comparison of the current function measured under Ar and under CO for **1a** and **2** shows that the two-electron pathway is favoured under CO. This was confirmed in the case of complex **2** by comparing its reduction peak current $[i_p^{red1}]$ with the peak current $[(i_p^a)^{ox}]$ of the one-electron oxidation of $[Fe_2Cp_2(CO)_2(\mu\text{-}SMe)_2]$[31–33] present in solution at the same concentration as **2**. The peak current ratio $[i_p^{red1}/(i_p^a)^{ox}]$ decreases from 1.5 (Ar) and ~1.7 (CO) to 1.2 (Ar or CO) upon increasing the scan rate from 0.02 V s^{-1} to 20 V s^{-1}. The effect of CO will be discussed below. Our results are consistent with

Table 1 Redox data[a] of the diiron complexes measured by CV under Ar (vitreous carbon electrode; potentials are in V *vs.* Fc^+/Fc)

Complex[b]	Solvent	v/V s^{-1}	$E_{1/2}^{red1}$/mV	ΔE_p^{red1}/mV	$E_{1/2}^{red2}$/mV	ΔE_p^{red2}/mV
$Fe_2(CO)_6\{\mu\text{-}SCH_2N\{R\}CH_2S\}$ **1a**	MeCN	0.2	−1.56	130	—	—
		40	−1.62	200	−1.60	650
R = CH_2CH_2OMe		60	−1.62	240	−1.61	690
$Fe_2(CO)_6\{\mu\text{-}SCH_2N(R)CH_2S\}$ **1b**	MeCN	0.2	−1.58	155	—	—
		10	−1.64	140	−1.63	410
R = ^{i}Pr		20	−1.65	140	−1.63	490
$Fe_2(CO)_6\{\mu\text{-}S(CH_2)_3S\}$ **2**	MeCN	0.2	−1.60	110	—	—
		20	−1.62	170	−1.80	870
		40	−1.62	230	−1.81	980
$Fe_2(CO)_5{}^1L_{NHC}\{\mu\text{-}S(CH_2)_3S\}$ **3a**	MeCN	0.2	−2.01	60	—	—
		40	−2.1	240	−2.1	590
		60	−2.1	280	−2.1	670
	THF	0.2	−2.16	130	—	—
	CH_2Cl_2	0.2	−2.24 (irr)	—	—	—
$Fe_2(CO)_5{}^2L_{NHC}\{\mu\text{-}S(CH_2)_3S\}$ **3b**	MeCN	0.2	−2.07 (irr)	—	—	—

[a] v, scan rate; ΔE_p, peak separation; irr, irreversible. [b] $^1L_{NHC}$ = 1,3-bis(methyl)-imidazol-2-ylidene; $^2L_{NHC}$ = 1,3-bis(2,4,6-trimethylphenyl)-imidazol-2-ylidene.

previous work on the reduction of complex **2**.[4a,18] However, our conclusion that the electrochemical reduction of **1** is an overall two-electron process at slow scan rate contradicts reports that analogues of **1** undergo one-electron reductions[8,9] under similar experimental conditions (solvent + supporting electrolyte, scan rate) to those used here.

The CV curves obtained for 0.04 V $s^{-1} \leq v \leq$ 40 V s^{-1} under Ar (Fig. 5) demonstrate that two separate one-electron steps can be observed for the reduction of **1** and **2** at fast scan rates (for **1b** see Fig. S3†). CVs of **1a** and **2** recorded under CO but under otherwise identical conditions are shown in Fig. S4.† That the second reduction peak (peak 2, i_p^{red2}, Fig. 5, S3 and S4†) is due to the reduction of the anion to the dianion rather than to formation of a daughter product is demonstrated by the increase of the peak current ratio [i_p^{red2}/i_p^{red1}] upon increasing v. Similarly, the oxidation peak of the dianion (peak 2′, Fig. 5, S3 and S4†) can be separated from that of the anion (peak 1′) at fast scan rates. It should be noted that the oxidation of the dianion takes place at a more positive potential than that of the anion (peaks 2′ and 1′, respectively) so that the latter is thermodynamically unstable at the potential of the oxidation of the dianion. Therefore, the oxidation peak 2′ corresponds to the two-electron oxidation of the dianion, eqn (1) [X = CH_2 or N(R), R = CH_2CH_2OMe or ^{i}Pr].

$$[Fe_2(CO)_6\{\mu\text{-}SCH_2XCH_2S\}]^{2-} - 2e \rightarrow [Fe_2(CO)_6\{\mu\text{-}SCH_2XCH_2S\}] \quad (1)$$

To the best of our knowledge, this is the first time that the two one-electron reduction steps of [$Fe_2(CO)_6$(μ-dithiolate)] compounds have been clearly separated. Very detailed analyses of electrochemical kinetic discrimination of the successive one-electron steps of an overall two-electron process (EE) have

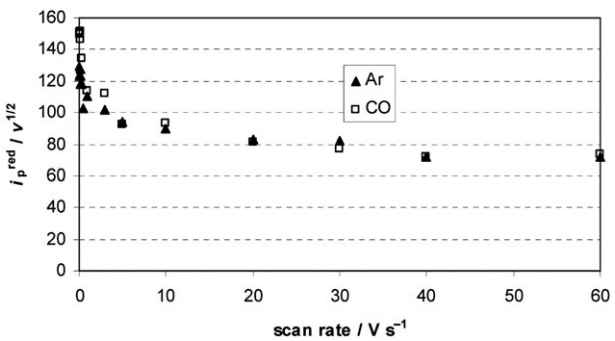

Fig. 4 Scan rate dependence of the current function for the reduction of [$Fe_2(CO)_6\{\mu\text{-}SCH_2N(CH_2CH_2OMe)CH_2S\}$] **1a** (1.3 mM) under Ar and under CO in MeCN–[NBu_4][PF_6] (vitreous carbon electrode).

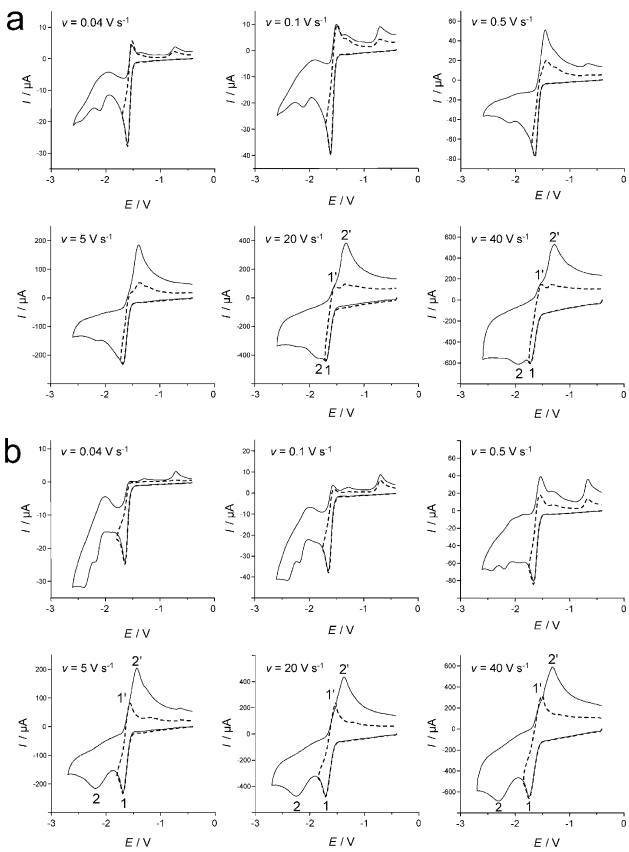

Fig. 5 Cyclic voltammetry of complexes (a) **1a** and (b) **2** in MeCN–[NBu_4][PF_6] under Ar at different scan rates (vitreous carbon electrode; potentials are in V *vs.* Fc^+/Fc).

been reported by several groups and parameters defining conditions under which wave-splitting is observable have been identified.[34,35] The central parameters are the separation of the formal potentials of the individual electron transfer steps (ΔE°), the relative rates of the heterogeneous electron transfers k_s, and the occurrence and rate of homogeneous electron transfer reactions. Wave-splitting was not observed for the two-electron reduction of $[Fe_2(CO)_6(\mu\text{-sdt})]$ or $[Fe_2(CO)_6(\mu\text{-bdt})]$ complexes for which the second heterogeneous rate constant k_s^{red2} was, respectively larger than, or similar to, k_s^{red1}.[7a,15]

In the present case, the second reduction step is much slower than the first one, as shown by the magnitude of the peak-to-peak separations, ΔE_p^{red2}: these increase from 460 mV (v = 20 V s^{-1}) to 690 mV (v = 60 V s^{-1}) for **1a**, from 490 mV (v = 20 V s^{-1}) to 720 mV (v = 60 V s^{-1}) for **1b** and from 540 mV (v = 3 V s^{-1}) to 1080 mV (v = 60 V s^{-1}) for **2**.[36] Previous studies have shown that disproportionation of the intermediate species in an overall two-electron transfer has a strong influence on the shape of CV curves[34,38] and on the extent of wave-splitting.[34] The redox potentials of the successive one-electron reductions of the complexes in MeCN–$[NBu_4][PF_6]$ (Table 1) lead to disproportionation constants, K_{disp}, of 4 ± 3 (**1a**); 2 ± 1 (**1b**) and $(2.4 \pm 2)\ 10^{-3}$ (**2**). At 298 K, the ratio of K_{disp} for **1a** : **2** ($4 : 2.4 \times 10^{-3}$) indicates a difference of approximately 18 kJ mol^{-1} in ΔG for the disproportionation reaction. The thermodynamically favourable disproportionation in **1a** and **1b** is confirmed by the presence of the oxidation peak of $\mathbf{1a}^{2-}$ and $\mathbf{1b}^{2-}$ (peak 2′, return scan) in the CVs limited to the first reduction (Fig. 5a, and S4a,† dotted line). Moreover, the persistence of this peak for scan rates up to 40 V s^{-1} demonstrates that the disproportionation of $\mathbf{1a}^{-}$ and $\mathbf{1b}^{-}$ are fast reactions. The rapid and thermodynamically favourable disproportionation of the one-electron reduced species therefore offers a simple explanation for the 2-electron nature of the reduction of **1a** and **1b**, where $K_{disp} > 1$. The basic reduction mechanism of **1** is summarised in the upper part of Scheme 3 where the heterogeneous steps are complemented by the disproportionation of the anion.

In contrast to the CV of **1a**, the oxidation peak 2′ is completely absent in the CVs of **2** recorded under the same conditions (Fig. 5b, dotted line), consistent with the much smaller disproportionation constant for **2** ($K_{disp} \ll 1$). Simple disproportionation of the anion cannot, therefore, account for the two-electron nature of the reduction of **2** at slow scan rates under Ar (Fig. S2†). We return to this point when we consider the nature of possible daughter products of the primary reduction.

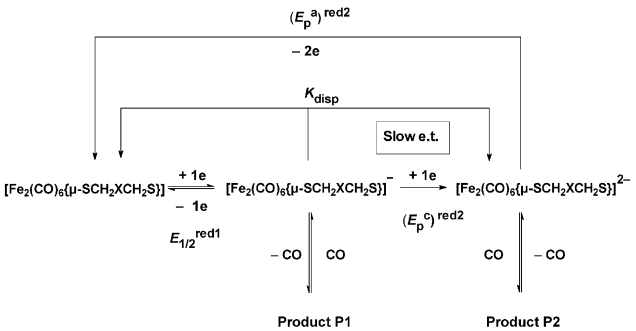

Scheme 3 X = CH_2 or NR; R = CH_2CH_2OMe or ^iPr (Product **P2** was not detected for X = N^{i}Pr).

2.2.2 Electronic structure of the reduced products. The previous paragraphs have highlighted both the rich electrochemistry of these diiron dithiolate complexes and the multiplicity of reduction products that can be formed under different conditions. The subtle differences between **1** and **2**, the most obvious of which is the change in disproportionation constant, K_{disp}, indicate that the substituent, R, on the amine bridgehead plays some role in the reaction. Overall two-electron transfers occur where the doubly reduced species is very stable relative to the anion, in which case the disproportionation constant, $K_{disp} > 1$. Typically, this situation arises where there is a substantial structural rearrangement that makes the transfer of a second electron thermodynamically more favourable than the first.[44–47] This is often the case when the LUMO of the complex (the SOMO of the reduced analogue) has strong σ antibonding character, leading to dramatic changes in bond length through the reduction process. Numerous calculations have confirmed that the LUMO in bimetallic complexes such as **1a**, **1b** and **2** has dominant M–M σ* character. Furthermore, the critical role of the bridging ligands in controlling the kinetics and thermodynamics of concerted two-electron transfer and metal–metal bond cleavage has been demonstrated for $[M_2(\mu\text{-}PPh_2)_2(CO)_8]^{0/2-}$ (M = Mo or W).[45e] Structural rearrangement therefore seems likely to be the cause of the two-electron behaviour observed for the reduction of **1** and **2**. The rather different electrochemical responses of **1a**, **1b** and **2** highlighted above, however, suggest that the extent of this rearrangement may depend on the nature of the R group.

In order to explore the nature of the reduction process in more detail, we have extended our density functional calculations on **1a** and **2** to include their 1- and 2-electron reduced analogues. Optimised structures of the neutral species, **2**, along with those of its 1- and 2-electron reduced analogues, are shown in Fig. 6, and key structural parameters for these and the corresponding species derived from reduction of **1a** and **2** are collected in Table 2. The electronic structure of complex **2** has been extensively studied by other groups, and our optimised structure is fully consistent with these earlier studies. In particular, the optimised Fe–Fe bond length of 2.51 A is very similar to those reported by Hall and co-workers.[19b,d]

The structural consequences of one- and two-electron reduction of **2** have also been discussed previously,[6b,23e] but we reiterate the key features here as they provide a logical reference point for the subsequent discussion of the role of the pendant CH_2CH_2OMe group in **1a**. The structural parameters summarised in Table 2 confirm that reduction of **2** does indeed populate the Fe–Fe σ* orbital, causing a significant elongation of both Fe–Fe (2.81 Å) and Fe–S (2.36 Å) bonds. The basic butterfly $Fe_2(\mu\text{-}SR)_2$ architecture is, however, retained, and the optimised structure of the core is very similar to that proposed by Borg *et al.* for the same species based on their infra-red spectroelectrochemical data.[4a] At the dianionic level ($\mathbf{2}^{2-}$) we have located three quite distinct local minima (**A**, **B** and **C**) on the potential energy surface, separated by less than 20 kJ mol^{-1}. Isomer **A** retains the butterfly structure

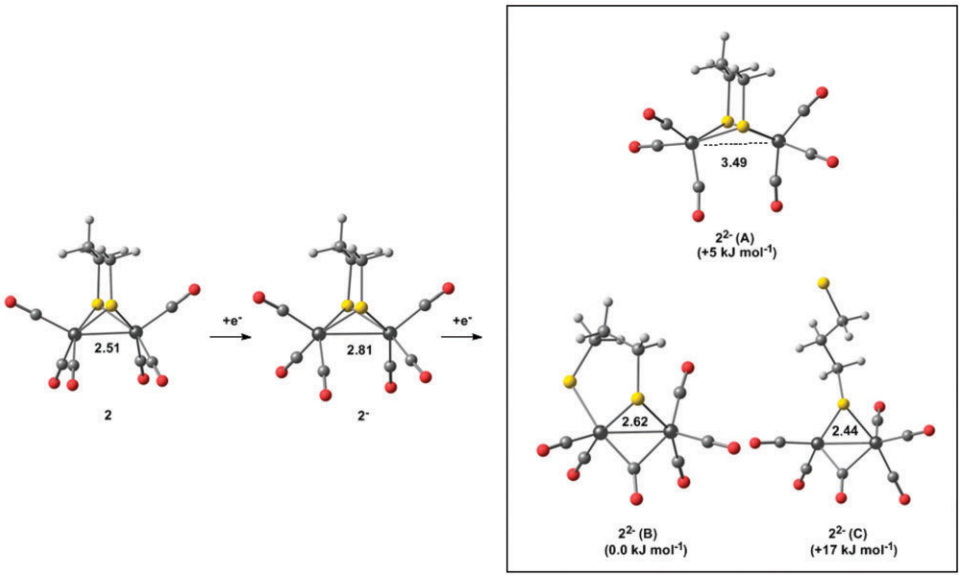

Fig. 6 Optimised structures of **2**, $\mathbf{2}^-$ and $\mathbf{2}^{2-}$ (isomers **A**, **B** and **C**).

of the $Fe_2(\mu\text{-SR})_2$ core found in **2** and $\mathbf{2}^-$, but the very long Fe–Fe distance (3.49 Å) is consistent with double occupation of the σ^* orbital. The core is therefore considerably flatter than in either the neutral or anionic structures, but the constraints of the chelating architecture prevent it from adopting the electronically preferred planar diamond structure. We have also located two further minima on the potential energy surface of $\mathbf{2}^{2-}$, corresponding to cleavage of either one (isomer **B**) or two (isomer **C**) Fe–S bonds. The tendency to cleave Fe–S bonds at the doubly reduced level is a natural consequence of the build up of negative charge at the metal core. The structure of isomer **C**, where one of the thiolate ligands is completely removed from the bimetallic core, is very similar to that proposed for $[Fe_2(CO)_6(\mu\text{-CO})\{\mu\text{-S}(CH_2)_3SH\}]^-$,[4a] albeit with one fewer carbonyl ligand. The nature of the metal–metal bonding in isomers **B** and **C** merits some comment. Cleavage of one or two Fe–S bonds in isomers **B** and **C**, respectively, reduces the total electron count at the metal core by two/four, hence requiring the formation of single (**B**) or double (**C**) Fe–Fe bonds to restore the 18-electron configuration at each metal. The very short Fe–Fe separation in isomer **C** (2.44 Å *cf.* 2.51 Å in **2**) provides clear evidence for some multiple character to the Fe–Fe bond. We find isomer **B** to be the global minimum in this case, lying 5 kJ mol^{-1} below the unrearranged structure, isomer **A**. Borg *et al.* computed a difference of 13 kJ mol^{-1} for the closely related species with one fewer CH_2 group in the dithiolate bridge.[6b]

Table 2 Key optimised bond lengths (Å) of **1a**, **2** and their one- and two-electron reduced derivatives, along with relative energies of the different isomers of the dianions

	Fe–Fe/Å	Fe–S/Å	E_{rel}/kJ mol^{-1}
2	2.51	2.31, 2.31, 2.31, 2.31	—
$\mathbf{2}^-$	2.81	2.36, 2.36, 2.36, 2.36	—
$\mathbf{2}^{2-}$ (A)	3.49	2.42, 2.43, 2.45, 2.45	+5
$\mathbf{2}^{2-}$ (B)	2.62	2.33, 2.38, 2.48, 4.27	0
$\mathbf{2}^{2-}$ (C)	2.44	2.30, 2.38. 7.11, 7.28	+17
1a	2.51	2.31, 2.31, 2.31, 2.31	—
$\mathbf{1a}^-$	2.81	2.36, 2.36, 2.36, 2.38	—
$\mathbf{1a}^{2-}$ (A)	3.49	2.40, 2.42, 2.43, 2.45	+31
$\mathbf{1a}^{2-}$ (B)	2.61	2.35, 2.38, 2.51, 4.26	0
$\mathbf{1a}^{2-}$ (C)	2.46	2.29, 2.38, 7.08, 7.42	+18

A survey of the potential energy surface of $\mathbf{1a}^-$ and $\mathbf{1a}^{2-}$ reveals a series of minima that are very similar in structure to those derived from **2**. In all cases the Fe···OMe distance remains long, indicating that coordination of the pendant arm (as observed in **1a–CO**) plays no role in stabilising the primary reduction products. In the context of the electrochemistry, the most significant observation is that the elongation of the Fe–Fe bond at the singly reduced level is identical for **1a** and **2**. Thus, although the stabilisation of the SOMO as a result of this elongation will undoubtedly play a role in lowering the potential of the second electron transfer (*i.e.* the tendency towards 2-electron behaviour in both **1a** and **2** at slow scan rates), it *cannot* account for the subtle differences between **1a** and **2**. At the dianionic level, however, differences between the two systems do emerge that may account for the contrasting electrochemical behaviour. For both $\mathbf{2}^{2-}$ and $\mathbf{1a}^{2-}$, isomer **B** is the most stable of the three, but in the former it lies only 5 kJ mol^{-1} below **A**, indicating that the driving force for Fe–S bond cleavage is relatively weak. In $\mathbf{1a}^{2-}$, in contrast, isomer **B** lies 31 kJ mol^{-1} below **A**, suggesting that cleavage of the Fe–S bonds is much more favourable in this case. Our calculations suggest that the pendant OMe group is entirely innocent in this process, and so the difference between **2** and **1a** must reflect the stabilising inductive effect of the nitrogen substituent in the bridge, a hypothesis that would also explain the similar electrochemical behaviour of **1a** and **1b**. Calculations on a generic model system with an NH group at the bridgehead confirm a strong (25 kJ mol^{-1}) preference for **B** over **A**.

Whatever the origin of the preference for Fe–S bond cleavage in **1a**, it is clear that the additional stabilisation of the dianion may have a significant impact on the

disproportionation of the anion, and hence on the electrochemical response. In the absence of any Fe–S bond cleavage at the dianionic level (*i.e.* considering only the butterfly isomer **A** in each redox state), the energies for the disproportionation reactions ($2\ X^{1-} \rightarrow X + X^{2-}$) are almost identical for **1a** and **2**. The additional stabilisation of $\mathbf{1a}^{2-}$ as a result of Fe–S bond cleavage (forming isomer **B**) makes the disproportionation more favourable by 31 kJ mol^{-1} (compared to a difference of 18 kJ mol^{-1} (ΔG) obtained from the electrochemical measurements). By Hammond's postulate, we would also anticipate that the greater driving force for Fe–S bond cleavage in $\mathbf{1a}^{2-}$ will reduce the barrier for rearrangement of isomer **A** to **B**, hence leading to the faster reduction of $\mathbf{1a}^{-}$ compared to $\mathbf{2}^{-}$, consistent with $k_s^{red2}(\mathbf{1}) > k_s^{red2}(\mathbf{2})$.[36]

2.2.3 The effect of CO on the reduction of 1 and 2. We have noted above that under Ar the reduction of the complexes with an azadithiolate bridge (**1a**, **1b**) is chemically more reversible than that of the propanedithiolate analogue (Fig. 3). Under CO, in contrast, significant return peaks even at slow scan rates indicate that the reduction of both **1a** and **2** becomes reversible. These results suggest that a reduced species undergoes CO loss, a well-known reaction for diiron carbonyl complexes.[3,4a,18,39] The daughter product (Product **P1** in Scheme 3) detected by a peak around −2.1 V (**1a**) or −2.2 V (**1b** and **2**) under Ar is absent under CO (compare Fig. 5†). The persistence of this peak for scan rates up to 10 V s^{-1} for **1a** confirms that reversible CO loss is a fast reaction.

We have already confirmed that the first reduction is a two-electron process at slow scan rates, so it is not clear, *a priori*, whether loss of CO occurs from the anion or the dianion. We favour the former for the following reasons:

(i) for **1**, both $(i_p^c)^{red1}$ and $(i_p^a)^{red1}$ measured at slow scan rates are larger under CO than under Ar.[40] The increase of $(i_p^c)^{red1}$ is consistent with more extensive disproportionation due to the stabilisation of $\mathbf{1}^{-}$ under CO.

(ii) for complex **2**, the kinetic stabilisation of the anion under CO is also revealed by the detection of its reduction peak around −1.9 V, which was absent under Ar (Fig. S4).

We therefore propose that the peak around −2.1 V (**1a**) or −2.2 V (**1b** and **2**) is due to reduction of a species, Product **P1**, derived from loss of a CO ligand from the anion, either directly or following subsequent reactions (Scheme 3).[41]

On the basis of infra-red spectroelectrochemical results, Borg *et al.* have proposed that CO loss from $\mathbf{2}^{-}$ is followed by a ligand redistribution reaction and recoordination of CO to form a dianionic species containing four metal centres (Fig. 7).[4a,6] This has been later confirmed by the full characterisation of this dianion generated by chemical reduction of **2**.[13b] The initial step in this process is clearly loss of CO to vacate a coordination site, so we have used DFT to explore the thermodynamic and structural effects of CO loss from the anions $\mathbf{1a}^{-}$ and $\mathbf{2}^{-}$. Optimised structures of the anions and their decarbonylated products ($\mathbf{1a}^{-}$**–CO**, $\mathbf{2}^{-}$**–CO**) are summarised in Fig. 7, along with the energies of CO loss. In $\mathbf{2}^{-}$, loss of CO results in a substantial redistribution of electron density, such that the additional electron moves from the Fe–Fe σ antibonding orbital into an orbital localised on the CO-deficient iron. The net result, in structural terms, is that the Fe–Fe bond contracts back to a value typical of an Fe–Fe single bond. The structural and energetic changes associated with CO loss from $\mathbf{1a}^{-}$ are very similar, with a significant contraction of the Fe–Fe bond. There is again no indication of coordination of the OMe group to the metal (Fe–O = 4.02 Å) but the pendant arm in **1a** does have a significant impact on the geometry at the CO-deficient iron centre. The CH_2CH_2OMe group lies directly over the vacant coordination site, with a relatively short Fe–(H–C) separation of 2.63 Å suggesting the presence of a weak stabilising interaction between the metal and alkyl chain. Whilst the preference for interaction with a C–H group, rather than OMe may seem somewhat surprising, it is consistent with the high electron density at the metal, and also explains the very similar behaviour of the ^{i}Pr analogue, **1b**, where a methyl group is similarly placed to block the vacant coordination site. In the context of the electrochemistry, the pendant arm in both **1a** and **1b** effectively blocks the dimerisation process that causes the loss of reversibility.

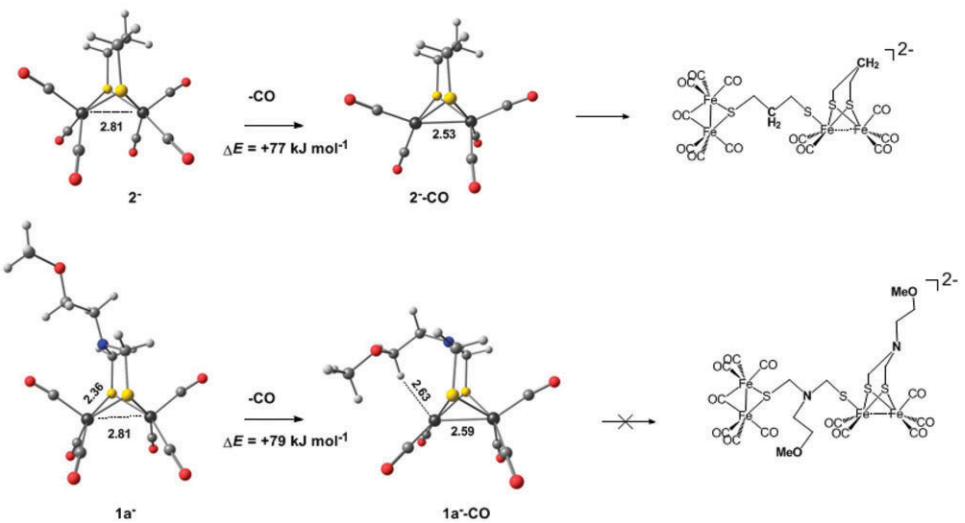

Fig. 7 Optimised structures of the anions, $\mathbf{1a}^{-}$ and $\mathbf{2}^{-}$, along with their decarbonylated products.

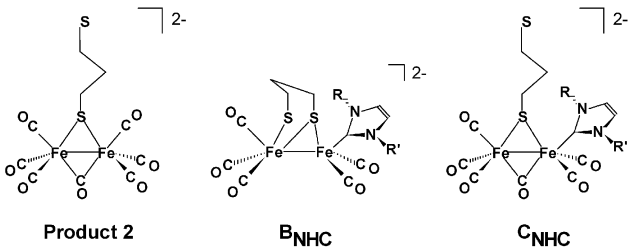

Scheme 4 Proposed structure of the doubly reduced carbonylated daughter products of **2** and **3a**.

In the CVs shown in Fig. 5, an additional quasi-reversible reduction peak around −2.4 V must also result from chemical reactions subsequent to the reduction of **1a** and **2** (this product was not detected in the accessible potential window in the case of **1b**). However, unlike the daughter peak at −2.1 V assigned to Product **P1** in Scheme 3, the peak at −2.4 V is observed under both Ar and CO, and can therefore reasonably be assigned as resulting from the decay of the dianion rather than anion (Product **P2** in Scheme 3). The fact that Product **P2** is observed under CO while the primary reduction maintains substantial chemical reversibility when the potential scan is reversed around −1.8 V (Fig. S4) suggests that the follow-up reaction is reversible. From the mechanism in Scheme 3, electrolysis of **1a** and **2** performed in the presence of CO should afford Product **P2** with a charge consumption of 2 F mol^{-1} **2**. Pickett and co-workers have shown that bulk electrolysis of **2** in MeCN under CO does indeed consume *ca.* 2 F mol^{-1} **2** to produce $[Fe_2(CO)_6(\mu\text{-}CO)\{\mu\text{-}S(CH_2)_3SH\}]^-$ [4a] where one of the two Fe–S bonds has been cleaved, and it seems likely that Product **P2** (Scheme 4) is analogous. The core structure of this species is very similar to isomer **C** of the dianion discussed in Fig. 6, except that it features an additional CO ligand. It seems reasonable, therefore, to suggest that excess CO drives the redox equilibria in Scheme 3 to the right by coordinating to the dianion. The net effect will therefore be to stabilise the dianion relative to the anion, and hence favour a two-, rather than one-electron process.

In summary, a two-electron reduction process requires that the dianion is relatively stable compared to the anion, allowing the second electron transfer to occur at or below the potential of the first. Our experiments and calculations have highlighted two ways in which this might happen. In $\mathbf{1a}^{2-}$, the presence of an electron-withdrawing NR substituent stabilises the negative charge by promoting cleavage of the Fe–S bond, and this is sufficient to drive a disproportionation reaction and hence two-electron reduction. In $\mathbf{2}^{2-}$, in contrast, cleavage of the Fe–S bonds is much less favourable unless excess CO is available to bind to the coordinatively unsaturated diiron core.

2.3 Electrochemical reduction of $[Fe_2(CO)_5L_{NHC}(\mu\text{-pdt})]$, 3a–b

[**a**: L_{NHC} = 1,3-bis(methyl)-imidazol-2-ylidene; **b**: L_{NHC} = 1,3-bis(2,4,6-trimethylphenyl)-imidzol-2-ylidene].

2.3.1 Reduction of 3 under Ar. Cyclic voltammetry of complex **3a** (Fig. 8a) shows partially reversible reduction ($E^{red}_{1/2}$ = −2.01 V, v = 0.2 V s^{-1}, Table 1)[7b] and oxidation ($E^{ox}_{1/2}$ = 0.11 V) processes in MeCN–$[NBu_4][PF_6]$ under Ar. The presence of several minor reduction and oxidation peaks (E^{red2}_p = −2.46 V; E^{ox}_p = −1.5 V; E^{ox}_p = −1.15 V) indicates that the reduction is followed by chemical reaction(s). The reduction of **3b** (E^{red}_p = −2.07 V) under the same conditions shows no sign of chemical reversibility at moderate scan rate, in agreement with the results reported by Darensbourg.[3f] The CV of **3a** was also briefly investigated in thf- and CH_2Cl_2–$[NBu_4][PF_6]$ (Fig. S5 and S6†). In thf, the electrochemical reduction of **3a** is similar to that in MeCN (Table 1; product peaks at E^{red}_p = −2.66 V; E^{ox}_p = −1.65 V; E^{ox}_p = −1.24 V), while the oxidation involves several steps, with only the first one partially reversible ($E^{ox}_{1/2}$ = 0.22 V) at v = 0.2 V s^{-1}. In CH_2Cl_2, the reduction is irreversible (Table 1; product peaks at $E^{red2}_p \sim -2.5$ V; $E^{ox}_p \sim -1.8$ V; E^{ox}_p = −1.14 V), but the oxidation is a fully reversible one-electron process on the CV time scale with $E^{ox}_{1/2}$ = 0.15 V (Fig. S6†). Comparison of the reduction peak current $(i^c_p)^{red1}$ with the current of the reversible one-electron oxidation of the complex, $[(i^c_p)^{red1}/(i^a_p)^{ox}$ = 1.95 for v = 0.05 V s^{-1}; 1.7 for v = 1 V s^{-1}], demonstrated unambiguously that the reduction involves the transfer of two electrons in CH_2Cl_2 at slow to moderate scan rates. This conclusion contradicts our previous report that the reduction of **3a** in MeCN–$[NBu_4][PF_6]$ was a one-, rather than two-electron process,[7b] so we decided to revisit the reduction of **3a** in MeCN by CV at variable scan rates to establish whether

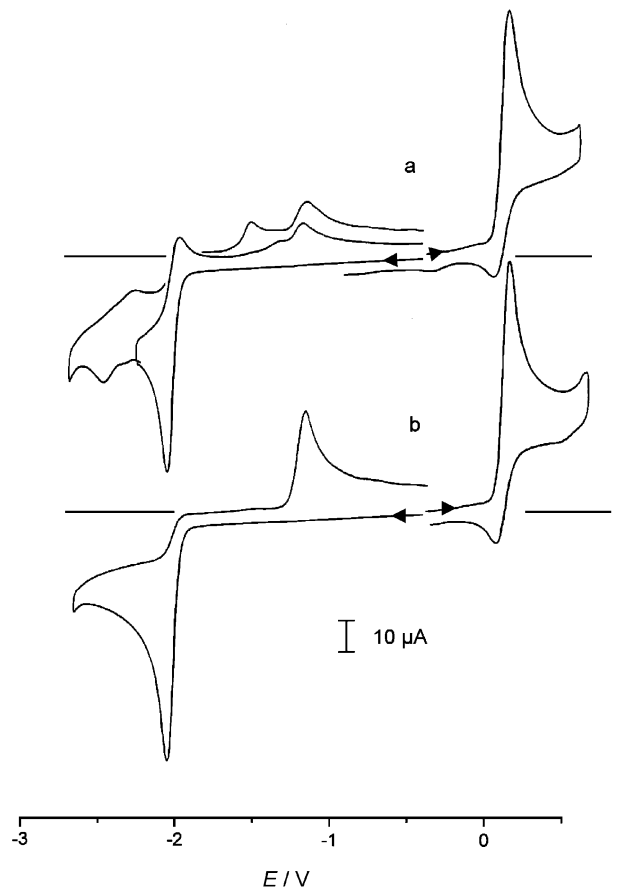

Fig. 8 Cyclic voltammetry of **3a** (a) under Ar, and (b) under CO in MeCN–$[NBu_4][PF_6]$ (vitreous carbon electrode; v = 0.2 V s^{-1}; potentials are in V *vs.* Fc^+/Fc).

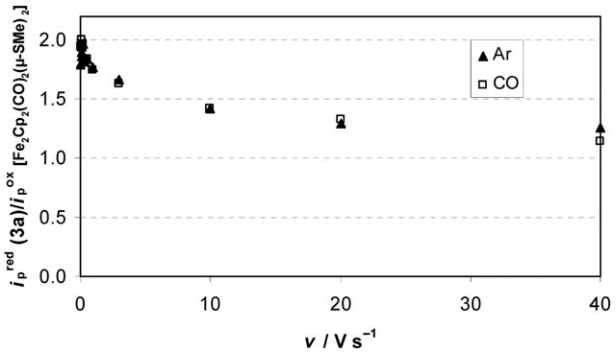

Fig. 9 Scan rate dependence of the ratio of the cyclic voltammetric reduction peak current of **3a** (1 mM) to the peak current of the one-electron oxidation of $[Fe_2Cp_2(CO)_2(\mu\text{-}SMe)_2]$ (1 mM) in MeCN–$[NBu_4][PF_6]$ (vitreous carbon electrode).

wave-splitting could be observed. The scan rate dependence of the current function $[i_p^{red1}/v^{1/2}]$, and the comparison of the current of the first reduction of **3a** with that of the first one-electron oxidation of an equimolar solution of $[Fe_2Cp_2(CO)_2(\mu\text{-}SMe)_2]$[32] at different scan rates (Fig. 9) demonstrate that at slow scan rate, the reduction of **3a** in MeCN–$[NBu_4][PF_6]$ is clearly a *two-electron* process (as is that of the analogue **3b**)[3f] but at faster rates two separate reduction steps can be detected, both with $E_{1/2}^{red} \sim -2.1$ V (Fig. 10). Thus wave-splitting does emerge in these systems, albeit much less distinctly than for **1a** and at faster scan rates. The scan rate dependence of the peak-to-peak separation for both reductions (Table 1) also suggests that the second electron transfer is again slower than the first one. Comparison with complex **2** shows that the substitution of a CO ligand by a N-heterocyclic carbene results in the expected negative shift of the redox potentials, but the potential shift is more pronounced for the first reduction step ($\Delta E_{1/2}^{red1} \sim 0.5$ V) than for the second one ($\Delta E_{1/2}^{red2} \sim 0.3$ V). Thus, the substituted anion is thermodynamically less stable than the parent and disproportionation of the anion, still detectable at $v = 60$ V s^{-1} (Fig. 10b, solid line) is responsible for the transition from a one- to a two-electron process, as illustrated by the scan rate dependence of the current function. The basic reduction mechanism of **3a** may also be represented as shown in Scheme 3 (with one of the CO ligands replaced by L_{NHC}).

2.3.2 Reduction of 3 under CO. The effect of CO on the CV of **3a** (Fig. 8b, S5b and S6b†) is strikingly different from that described above for **1** and **2**. In the all-carbonyl species, an atmosphere of CO made the reduction more reversible but in **3a** precisely the opposite is found and the reduction becomes totally irreversible ($E_p^{red} = -2.04$ V in MeCN). The product peaks observed under Ar at −2.46 V and −1.5 V for **3a**, and at $E_{1/2} = -2.4$ V and $E_p^{ox} = -1.53$ V for **3b**, are absent under CO and only a single oxidation peak is observed on the return scan at −1.15 V (**3a**) (Fig. 8b) or −1.32 V (**3b**). The comparison of the CVs of **3a** recorded at fast scan rates under Ar and under CO demonstrates that the CO effect arises from the reaction of the dianion with CO, since the oxidation peak of $\mathbf{3a}^{2-}$ (peak 2′) is replaced by one at −1.15 V when CO is present (Fig. 10). This reaction is quite fast since it is still observed at scan rates

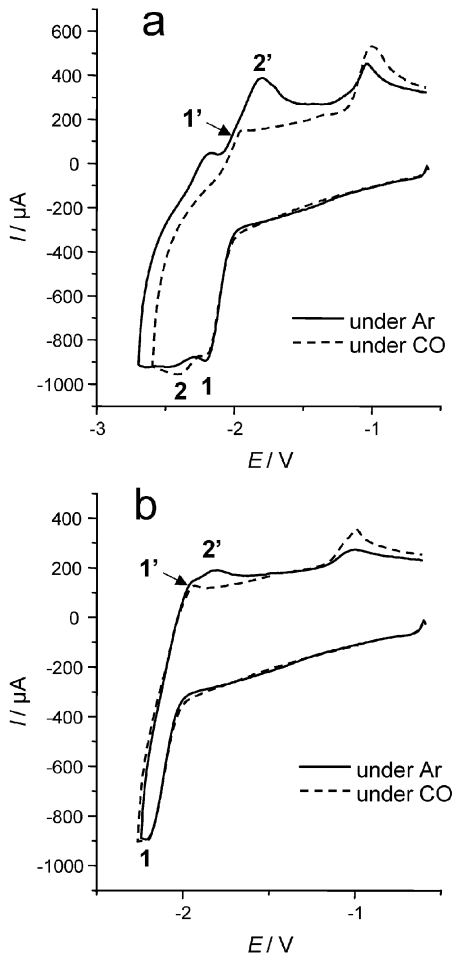

Fig. 10 Cyclic voltammetry of **3a** (1.1 mM) in MeCN–$[NBu_4][PF_6]$ under Ar (solid line) and under CO (broken line); in panel a the potential scan covers both reduction events, and only the first one in panel b ($v = 60$ V s^{-1}; vitreous carbon electrode; potentials are in V *vs.* Fc^+/Fc).

up to 60 V s^{-1}. The *removal* of the dianion $\mathbf{3a}^{2-}$ under CO suggests that coordination of CO must be involved, which in turn suggests the presence of a vacant coordination site at the metal in the doubly reduced species. We can eliminate dissociation of the NHC ligand as a potential source of the vacant site because the oxidation peak observed on the return scan under CO occurs at different potentials for **3a** (–1.15 V) and for **3b** (–1.32 V), indicating that the NHC ligand remains attached to the metal core. Alternatively, two-electron reduction of the NHC-substituted complexes **3a** and **3b** may result in the cleavage of one or more Fe–S bonds, in a process precisely analogous to that which generates isomers **B** and **C** in the all-carbonyl species (Fig. 6). In the presence of excess CO, coordination of an additional ligand to the coordinatively unsaturated intermediate obtained by reduction of **3a** and **3b** would lead to compounds $\mathbf{B_{NHC}}$ or $\mathbf{C_{NHC}}$ shown in Scheme 4, where $\mathbf{C_{NHC}}$ is a substituted analogue of the $[Fe_2(CO)_6\{\mu\text{-}CO\}(\mu\text{-}S(CH_2)_3SH\}]^-$ species observed by Borg *et al.* upon bulk electrolysis of **2**.[4a]

The very different behaviour of **3a** and **2** may result from a combination of factors: first, the formation of the NHC

analogue of Product **P1** would be hindered if the CO ligands are less labile in the $[Fe_2(CO)_5L_{NHC}(\mu\text{-pdt})]^-$ anion than in its hexacarbonyl parent; secondly, it is expected that the Fe–S bonds in the $[Fe_2(CO)_5L_{NHC}(\mu\text{-pdt})]^{2-}$ dianion will cleave more easily than those in $\mathbf{2}^{2-}$, and the subsequent binding of CO to the more electron-rich site appears to be irreversible.

Conclusion

In this paper we have shown that the two one-electron reduction steps of different $[Fe_2(CO)_5L(\mu\text{-dithiolate})]$ complexes are discernible by cyclic voltammetry at fast scan rates. The nature of the S-to-S link affects the reduction of the hexacarbonyl complexes in that the potentials of the redox steps are inverted only for those containing an azadithiolate bridge so that E° (or $E_{1/2}$) for the second reduction is less negative than that of the first, while it is more negative for the pdt complex. Therefore, the reduction of $[Fe_2(CO)_6\{\mu\text{-}SCH_2N(R)CH_2S\}]$ tends towards a two-electron process at lower scan rates owing to the disproportionation of the anion. Density functional theory suggests that the addition of the first electron leads to a substantial lengthening of the Fe–Fe bond, but 2-electron reduction gives two structures with very similar energy, where either the Fe–Fe or an Fe–S bond is cleaved. The presence of the azadithiolate bridge promotes cleavage of the Fe–S bond, and this structural reorganisation may provide the driving force for the disproportionation reaction.

The substitution of a N-heterocyclic carbene ligand for CO in the complex with a propanedithiolate bridge was found to alter the reduction both thermodynamically and kinetically. The substitution leads to a negative shift of the redox potentials that is larger for the first reduction than for the second, and thus to a thermodynamically less stable anion for the substituted derivative. The two-electron reduction of the NHC-substituted complex **3a** is thus due to disproportionation of the anion rather than to simultaneous electron uptake by the Fe–Fe core and the NHC ligand as in the case of the analogue **3b**.[3f] On the other hand, the increased electron density at the metal core in the $[Fe_2(CO)_5L_{NHC}(\mu\text{-pdt})]^{n-}$ species makes the CO ligands less labile in the anion and facilitates Fe–S bond cleavage in the dianion as well as the subsequent binding of a CO ligand.

The overall two-electron reduction of azadithiolate hexacarbonyl complexes and the ensuing Fe–S bond cleavage may have consequences on the mechanisms of proton reduction by these compounds. Further studies are in progress in our laboratory to examine this question.

Experimental section

Methods and materials

All the experiments were carried out under an inert atmosphere, using Schlenk techniques for the syntheses. Tetrahydrofuran (THF) was purified as described previously.[48] Acetonitrile (Merck, HPLC grade) was used as received. $[Fe_2(\mu\text{-}S)_2(CO)_6]$ was prepared according to reported methods.[49,50] *N*,*N*-di(chloromethyl)-2-methoxyethylamine and *N*,*N*-di(chloromethyl)-2-isopropyl amine were obtained from reaction of paraformaldehyde with either 2-methoxyethylamine or isopropylamine, followed by chlorination with thionyl chloride, according to a reported procedure.[5a] All other chemicals were used as purchased (Sigma-Aldrich).

The preparation and the purification of the supporting electrolyte $[NBu_4][PF_6]$ were described previously.[48] The electrochemical equipment consisted in a GCU potentiostat (Tacussel/Radiometer) driven by a PAR 175 Universal Programmer, CV traces were recorded with a SEFRAM TGM 164 X-Y recorder. Fast scan CV were obtained with a PGSTAT 12 or a μ-AUTOLAB (Type III) driven by a GPES software. All the potentials (text, tables, figures) are quoted against the ferrocene–ferrocenium couple; ferrocene was added as an internal standard at the end of the experiments. 1H NMR spectra were recorded on a Bruker AC300 spectrophotometer. Shifts are relative to tetramethylsilane as an internal reference. The infrared spectra were recorded on a Nicolet Nexus Fourier transform spectrometer. Chemical analyses were made by the Service de Microanalyses I.C.S.N., Gif sur Yvette (France).

Syntheses

Synthesis of $[Fe_2(CO)_6\{\mu\text{-}SCH_2N(CH_2CH_2OCH_3)CH_2S\}]$ (1a). The addition of 2 molar equivalents of $LiBEt_3H$ (6 mL, 6 mmol) to a solution of $[Fe_2(\mu\text{-}S)_2(CO)_6]$ (1 g, 2.9 mmol) at −78 °C gave a green solution of the dianion $[Fe_2(\mu\text{-}S)_2(CO)_6]^{2-}$. To this was added dropwise a THF solution (10 mL) of *N*,*N*-di(chloromethyl)-2-methoxyethylamine $(ClCH_2)_2N(CH_2)_2OCH_3$ (0.525 g, 3.1 mmol). The reaction mixture turned red and was stirred for 2 h at room temperature. Solvent was removed under vacuum, leaving a red oil which was extracted with 3 × 50 mL of Et_2O. The combined solution was evaporated to dryness under vacuum. The crude product was chromatographed on silica gel. An orange band was eluted with a dichloromethane–hexane (25 : 75) mixture and gave only the starting material. A second red band collected with dichloromethane gave compound **1**. 100 mL of hexane were added to compound **1** and the solution obtained was concentrated to 5 mL under vacuum. A red powder of complex **1a** (0.57 g, yield 44%) was recovered after filtration.

N,N-Di(chloromethyl)-2-methoxyethylamine. ^1H NMR (300 MHz, $CDCl_3$): δ 5.25 (s, 4H, $N(CH_2)_2S_2$), 3.59 (t, J_{HH} = 5.1 Hz, 2H, $NCH_2CH_2OCH_3$), 3.37 (s, 3H, OCH_3), 3.18 ppm (t, J_{HH} = 5.1 Hz, 2H, $NCH_2CH_2OCH_3$).

1a. ^1H NMR (300 MHz, $CDCl_3$): δ 3.64 (s, 4H, $N(CH_2)_2S_2$), 3.23 (t, J_{HH} = 5.4 Hz, 2H, $NCH_2CH_2OCH_3$), 3.20 (s, 3H, OCH_3), 2.86 (t, J_{HH} = 5.4 Hz, 2H, $NCH_2CH_2OCH_3$). IR (CH_2Cl_2): ν_{CO} = 2073, 2034, 1996 cm^{-1}. Anal. Calcd for $C_{11}H_{11}Fe_2NO_7S_2$: C, 29.69; H, 2.49; N, 3.15. Found: C, 29.42; H, 2.55; N, 3.29.

Synthesis of $[Fe_2(CO)_6\{\mu\text{-}SCH_2N(^iPr)CH_2S\}]$ (1b). To a solution of $[Fe_2(\mu\text{-}S)_2(CO)_6]$ (0.5 g, 1.45 mmol) in tetrahydrofuran (50 mL) was added dropwise 2 equiv. of $LiBEt_3H$ (2.9 mL, 2.9 mmol) at −78 °C. After 30 min stirring, the solution turned from red to green. To this was added at −78 °C a solution of chloramine (0.272 g, 1.74 mmol) in

tetrahydrofuran (5 mL). The reaction mixture turned red and was stirred for 2 h until the temperature of the solution raised to 25 °C. Solvent was then removed under vacuum, giving a red oil that was extracted with 3 × 15 mL of diethylether. The combined extracts were evaporated to dryness, and the crude product, dissolved in hexane, was chromatographed on silica gel. Elution with hexane–dichloromethane (9 : 1) gave a red band, that after evaporation of the volatiles afforded a brick-red powder of complex **1b** (125 mg, 20% yield).

N,N-Di(chloromethyl)-2-isopropylamine. ^{1}H NMR (300 MHz, $CDCl_3$): δ 5.30 (s, 4H, $N(CH_2)_2S_2$), 3.41 (spt, J_{HH} = 6.6 Hz, 1H, $NCH(CH_3)_2$), 1.27 ppm (d, J_{HH} = 6.6 Hz, 6H, $NCH(CH_3)_2$).

1b. ^{1}H NMR (300 MHz, $CDCl_3$): δ 3.22 (s, 4H, $N(CH_2)_2S_2$), 2.82 (spt, J_{HH} = 7.4 Hz, 1H, $NCH(CH_3)_2$), 0.92 ppm (d, J_{HH} = 7.4 Hz, 6H, $NCH(CH_3)_2$). IR (CH_2Cl_2): ν_{CO} = 2073(w), 2034(s), 1996(s) cm^{-1}. Anal. Calcd for $C_{11}H_{11}Fe_2NO_6S_2$: C, 30.79; H, 2.58; N, 3.26. Found: C, 30.37; H, 2.62; N, 3.16.

Crystal structure analysis of 1a

Crystal data. $C_{11}H_{11}Fe_2NO_7S_2$, M = 445.03, triclinic, space group $P\bar{1}$ (no. 2), a = 7.4291(4), b = 9.8933(6), c = 11.8779(7) Å, α = 73.116(3), β = 78.757(3), γ = 86.088(4)°, U = 819.3(1) Å^3, Z = 2, ρ_{calcd} = 1.804 g cm^{-3}, T = 100 K. Mo-K$_\alpha$ X-rays, λ = 0.71073 Å, μ = 2.057 mm^{-1}, θ_{max} = 30.1°, red plate 0.50 × 0.30 × 0.10 mm, 14 673 intensity measurements from thick-slice ϕ or ω scans, transmission factors 0.614–0.815, all 4735 unique reflections (R_{int} = 0.06) gave $R(F)$ = 0.039, w$R(F^2)$ = 0.080 when 209 parameters were refined on F^2, $|\Delta\rho| < 0.58$ e Å^{-3}, riding model for H atoms, only CH_3 orientation refined.[51]‡

Details of calculations. All calculations were performed with Gaussian 03 package,[52] using the hybrid B3LYP functional[53] in conjunction with the SDD basis set and associated effective core potential for Fe[54] and 6-31G(d,p) basis sets for all other atoms. Fully unconstrained geometry optimisations were performed and the resultant stationary points were confirmed as minima through vibrational analysis.

Acknowledgements

This work was supported by CNRS (France, Programme "Energie", PRI-4.1) and ANR (Programme "PhotoBioH2"). EPSRC (UK), Université de Bretagne Occidentale and Glasgow University are acknowledged for financial support.

References

1 (*a*) J. W. Peters, W. N. Lanzilotta, B. J. Lemon and L. C. Seefeldt, *Science*, 1998, **282**, 1853–1858; (*b*) Y. Nicolet, C. Piras, P. Legrand, C. E. Hatchikian and J. C. Fontecilla-Camps, *Structure*, 1999, **7**, 13–23; (*c*) Y. Nicolet, A. L. de Lacey, X. Vernede, V. M. Fernandez, C. E. Hatchikian and J. C. Fontecilla-Camps, *J. Am. Chem. Soc.*, 2001, **123**, 1596–1602; (*d*) B. J. Lemon and J. W. Peters, *Biochemistry*, 1999, **38**, 12969–12973.

2 For recent reviews, see: (*a*) I. P. Georgakaki, L. M. Thomson, E. J. Lyon, M. B. Hall and M. Y. Darensbourg, *Coord. Chem. Rev.*, 2003, **238–239**, 255–266; (*b*) M. Y. Darensbourg, E. J. Lyon, X. Zhao and I. P. Georgakaki, *Proc. Natl. Acad. Sci. U. S. A.*, 2003, **100**, 3683–3688; (*c*) D. J. Evans and C. J. Pickett, *Chem. Soc. Rev.*, 2003, **32**, 268–275; (*d*) T. B. Rauchfuss, *Inorg. Chem.*, 2004, **43**, 14–26; (*e*) L.-C. Song, *Acc. Chem. Res.*, 2005, **38**, 21–28; (*f*) V. Artero and M. Fontecave, *Coord. Chem. Rev.*, 2005, **249**, 1518–1535; (*g*) S. P. Best, *Coord. Chem. Rev.*, 2005, **249**, 1536–1554; (*h*) M. Bruschi, G. Zampella, P. Fantucci and L. De Gioia, *Coord. Chem. Rev.*, 2005, **249**, 1620–1640; (*i*) X. Liu, S. K. Ibrahim, C. Tard and C. J. Pickett, *Coord. Chem. Rev.*, 2005, **249**, 1641–1652; (*j*) L. Sun, B. Akermark and S. Ott, *Coord. Chem. Rev.*, 2005, **249**, 1653–1663; (*k*) J.-F. Capon, F. Gloaguen, P. Schollhammer and J. Talarmin, *Coord. Chem. Rev.*, 2005, **249**, 1664–1676; (*l*) P. Vignais, *Coord. Chem. Rev.*, 2005, **249**, 1677–1690, and references cited therein.

3 (*a*) D. Chong, I. P. Georgakaki, R. Mejia-Rodriguez, J. Sanabria-Chinchilla, M. P. Soriaga and M. Y. Darensbourg, *Dalton Trans.*, 2003, 4158–4163; (*b*) E. J. Lyon, I. P. Georgakaki, J. H. Reibenspies and M. Y. Darensbourg, *Angew. Chem., Int. Ed.*, 1999, **38**, 3178–3180; (*c*) E. J. Lyon, I. P. Georgakaki, J. H. Reibenspies and M. Y. Darensbourg, *J. Am. Chem. Soc.*, 2001, **123**, 3268–3278; (*d*) X. Zhao, I. P. Georgakaki, M. L. Miller, R. Mejia-Rodriguez, C.-H. Chiang and M. Y. Darensbourg, *Inorg. Chem.*, 2002, **41**, 3917–3928; (*e*) R. Mejia-Rodriguez, D. Chong, J. H. Reibenspies, M. P. Soriaga and M. Y. Darensbourg, *J. Am. Chem. Soc.*, 2004, **126**, 12004–12014; (*f*) J. W. Tye, J. Lee, H.-W. Wang, R. Mejia-Rodriguez, J. H. Reibenspies, M. B. Hall and M. Y. Darensbourg, *Inorg. Chem.*, 2005, **44**, 5550–5552.

4 (*a*) S. J. Borg, T. Behrsing, S. P. Best, M. Razavet, X. Liu and C. J. Pickett, *J. Am. Chem. Soc.*, 2004, **126**, 16988–16999; (*b*) M. Razavet, S. C. Davies, D. L. Hughes, J. E. Barclay, D. J. Evans, S. A. Fairhurst, X. Liu and C. J. Pickett, *Dalton Trans.*, 2003, 586–595; (*c*) A. Le Cloirec, S. P. Best, S. Borg, S. C. Davies, D. J. Evans, D. L. Hughes and C. J. Pickett, *Chem. Commun.*, 1999, 2285–2286; (*d*) M. Razavet, S. C. Davies, D. L. Hughes and C. J. Pickett, *Chem. Commun.*, 2001, 847–848; (*e*) M. Razavet, S. J. Borg, S. J. George, S. P. Best, S. A. Fairhurst and C. J. Pickett, *Chem. Commun.*, 2002, 700–701; (*f*) S. J. George, Z. Cui, M. Razavet and C. J. Pickett, *Chem.–Eur. J.*, 2002, **8**, 4037–4046.

5 (*a*) J. D. Lawrence, H. Li and T. B. Rauchfuss, *Chem. Commun.*, 2001, 1482–1483; (*b*) M. Schmidt, S. M. Contakes and T. B. Rauchfuss, *J. Am. Chem. Soc.*, 1999, **121**, 9736–9737; (*c*) J. D. Lawrence, H. Li, T. B. Rauchfuss, M. Bénard and M.-M. Rohmer, *Angew. Chem., Int. Ed.*, 2001, **40**, 1768–1771; (*d*) H. Li and T. B. Rauchfuss, *J. Am. Chem. Soc.*, 2002, **124**, 726–727; (*e*) F. Gloaguen, J. D. Lawrence and T. B. Rauchfuss, *J. Am. Chem. Soc.*, 2001, **123**, 9476–9477; (*f*) F. Gloaguen, J. D. Lawrence, M. Schmidt, S. R. Wilson and T. B. Rauchfuss, *J. Am. Chem. Soc.*, 2001, **123**, 12518–12527; (*g*) F. Gloaguen, J. D. Lawrence, T. B. Rauchfuss, M. Bénard and M.-M. Rohmer, *Inorg. Chem.*, 2002, **41**, 6573–6582; (*h*) C. A. Boyke, T. B. Rauchfuss, S. R. Wilson, M.-M. Rohmer and M. Bénard, *J. Am. Chem. Soc.*, 2004, **126**, 15151–15160; (*i*) J. D. Lawrence, T. B. Rauchfuss and S. R. Wilson, *Inorg. Chem.*, 2002, **41**, 6193–6195.

6 (*a*) M. H. Cheah, S. J. Borg, M. I. Bondin and S. P. Best, *Inorg. Chem.*, 2004, **43**, 5635–5644; (*b*) S. J. Borg, J. W. Tye, M. B. Hall and S. P. Best, *Inorg. Chem.*, 2007, **46**, 384–394; (*c*) M. H. Cheah, S. J. Borg and S. P. Best, *Inorg. Chem.*, 2007, **46**, 1741–1750.

7 (*a*) J.-F. Capon, F. Gloaguen, P. Schollhammer and J. Talarmin, *J. Electroanal. Chem.*, 2004, **566**, 241–247; (*b*) J.-F. Capon, S. El Hassnaoui, F. Gloaguen, P. Schollhammer and J. Talarmin, *Organometallics*, 2005, **24**, 2020–2022; (*c*) P. Das, J.-F. Capon, F. Gloaguen, F. Y. Pétillon, P. Schollhammer and J. Talarmin, *Inorg. Chem.*, 2004, **43**, 8203–8205; (*d*) J.-F. Capon, F. Gloaguen, P. Schollhammer and J. Talarmin, *J. Electroanal. Chem.*, 2006, **595**, 47–52.

8 (*a*) S. Ott, M. Kritikos, B. Åkermark, L. Sun and R. Lomoth, *Angew. Chem., Int. Ed.*, 2004, **43**, 1006–1009; (*b*) T. Liu, M. Wang, Z. Shi, H. Cui, W. Dong, J. Chen, B. Åkermark and L. Sun, *Chem.–Eur. J.*, 2004, **10**, 4474–4479; (*c*) W. Gao, J. Liu, C. Ma, L. Weng, K. Jin, C. Chen, B. Åkermark and L. Sun, *Inorg. Chim. Acta*, 2006, **359**, 1071–1080; (*d*) Z. Wang, J. Liu, C. He, S. Jiang, B. Åkermark and L. Sun, *Inorg. Chim. Acta*, 2007, **360**,

‡ CCDC reference number 244692. For crystallographic data in CIF or other electronic format see DOI: 10.1039/b709273c

2411–2419; (*e*) F. Wang, M. Wang, X. Liu, K. Jin, W. Dong, G. Li, B. Åkermark and L. Sun, *Chem. Commun.*, 1999, **1**, 3221–3222; (*f*) S. Ott, M. Kritikos, B. Åkermark and L. Sun, *Angew. Chem., Int. Ed.*, 2003, **42**, 3285–3288; (*g*) S. Jiang, J. Liu, Y. Shi, Z. Wang, B. Åkermark and L. Sun, *Dalton Trans.*, 2007, 896–902, and references therein.

9 (*a*) S. Jiang, J. Liu and L. Sun, *Inorg. Chem. Commun.*, 2006, **9**, 290–292; (*b*) H.-G. Cui, M. Wang, W.-B. Dong, L.-L. Duan and L.-C. Sun, *Polyhedron*, 2007, **26**, 904–910; (*c*) L. Duan, M. Wang, P. Li, Y. Na, N. Wang and L. Sun, *Dalton Trans.*, 2007, 1277–1283.

10 (*a*) L. Schwartz, J. Ekström, R. Lomoth and S. Ott, *Chem. Commun.*, 2006, 4206–4208; (*b*) L. Schwartz, G. Eilers, L. Eriksson, A. Gogoll, R. Lomoth and S. Ott, *Chem. Commun.*, 2006, 520–522.

11 (*a*) J. Hou, X. Peng, J. Liu, Y. Gao, X. Zhao, S. Gao and K. Han, *Eur. J. Inorg. Chem.*, 2006, 4679–4686; (*b*) J. Hou, X. Peng, Z. Zhou, S. Sun, X. Zhao and S. Gao, *J. Organomet. Chem.*, 2006, **691**, 4633–4640.

12 (*a*) L.-C. Song, Z.-Y. Yang, H.-Z. Bian and Q.-M. Hu, *Organometallics*, 2004, **23**, 3082–3084; (*b*) L.-C. Song, M.-Y. Tang, F.-H. Su and Q.-M. Hu, *Angew. Chem., Int. Ed.*, 2006, **45**, 1130–1333.

13 (*a*) J. L. Nehring and D. M. Heinekey, *Inorg. Chem.*, 2003, **42**, 4288–4292; (*b*) I. Aguirre de Carcer, A. DiPasquale, A. L. Rheingold and D. M. Heinekey, *Inorg. Chem.*, 2006, **45**, 8000–8002.

14 G. Hogarth and I. Richards, *Inorg. Chem. Commun.*, 2007, **10**, 66–70.

15 J. Windhager, M. Rudolph, S. Bräutigam, H. Görls and W. Weigand, *Eur. J. Inorg. Chem.*, 2007, 2748–2760.

16 R. E. Dessy, F. E. Stary, R. B. King and M. Waldrop, *J. Am. Chem. Soc.*, 1966, **88**, 471–476.

17 R. Mathieu, R. Poilblanc, P. Lemoine and M. Gross, *J. Organomet. Chem.*, 1979, **165**, 243–252.

18 (*a*) A. Darchen, H. Mousser and H. Patin, *J. Chem. Soc., Chem. Commun.*, 1988, 968–970; (*b*) H. Mousser, *Thesis*, University of Rennes, France, 1987.

19 (*a*) H.-J. Fan and M. B. Hall, *J. Am. Chem. Soc.*, 2001, **123**, 3828–3829; (*b*) Z. Cao and M. B. Hall, *J. Am. Chem. Soc.*, 2001, **123**, 3734–3742; (*c*) J. W. Tye, M. Y. Darensbourg and M. B. Hall, *J. Mol. Struct.: THEOCHEM*, 2006, **771**, 123–128; (*d*) J. W. Tye, M. Y. Darensbourg and M. B. Hall, *Inorg. Chem.*, 2006, **45**, 1552–1559.

20 S. Motiu, D. Dogaru and V. Gogonea, *Int. J. Quantum Chem.*, 2006, **107**, 1248–1252.

21 M.-H. Baik, T. Ziegler and C. K. Schauer, *J. Am. Chem. Soc.*, 2000, **122**, 9143–9154.

22 (*a*) Z.-P. Liu and P. Hu, *J. Am. Chem. Soc.*, 2002, **124**, 5175–5182; (*b*) Z.-P. Liu and P. Hu, *J. Chem. Phys.*, 2002, **117**, 8177–8180.

23 (*a*) M. Bruschi, P. Fantucci and L. De Gioia, *Inorg. Chem.*, 2002, **41**, 1421–1429; (*b*) M. Bruschi, P. Fantucci and L. De Gioia, *Inorg. Chem.*, 2003, **42**, 4773–4781; (*c*) G. Zampella, M. Bruschi, P. Fantucci, M. Razavet, C. J. Pickett and L. De Gioia, *Chem.–Eur. J.*, 2005, **11**, 509–520; (*d*) G. Zampella, C. Greco, P. Fantucci and L. De Gioia, *Inorg. Chem.*, 2006, **45**, 4109–4118; (*e*) C. Greco, G. Zampella, L. Bertini, M. Bruschi, P. Fantucci and L. De Gioia, *Inorg. Chem.*, 2007, **46**, 108–116; (*f*) A. K. Justice, G. Zampella, L. De Gioia, T. B. Rauchfuss, J. I. van der Vlugt and S. R. Wilson, *Inorg. Chem.*, 2007, **46**, 1655–1664.

24 (*a*) T. Zhou, Y. Mo, A. Liu, Z. Zhou and K. R. Tsai, *Inorg. Chem.*, 2004, **43**, 923–930; (*b*) T. Zhou, Y. Mo, Z. Zhou and K. Tsai, *Inorg. Chem.*, 2005, **44**, 4941–4946.

25 (*a*) A. T. Fiedler and T. C. Brunold, *Inorg. Chem.*, 2005, **44**, 1794–1809; (*b*) A. T. Fiedler and T. C. Brunold, *Inorg. Chem.*, 2005, **44**, 9322–9334.

26 (*a*) S. Zilberman, E. I. Stiefel, M. H. Cohen and R. Car, *J. Phys. Chem. B*, 2006, **110**, 7049–7057; (*b*) S. Zilberman, E. I. Stiefel, M. H. Cohen and R. Car, *Inorg. Chem.*, 2007, **46**, 1153–1161.

27 F. H. Allen, *Acta Crystallogr., Sect. B: Struct. Sci.*, 2002, **58**, 380–388.

28 The parameters i_p and E_p are, respectively the peak current and the peak potential of a redox process; $E_{1/2} = (E_p^a + E_p^c)/2$; E_p^a, i_p^a and E_p^c, i_p^c are, respectively the potential and the current of the anodic and of the cathodic peak of a reversible process; $\Delta E_p = E_p^a - E_p^c$; k_s (in cm s^{-1}) is the rate constant of the heterogeneous electron-transfer. CV stands for cyclic voltammetry; v (V s^{-1}) is the scan rate in CV experiments.

29 The peak current ratio was measured according to the procedure of Nicholson, see ref. 30.

30 R. S. Nicholson, *Anal. Chem.*, 1966, **38**, 1406.

31 P. Madec, K. W. Muir, F. Y. Pétillon, R. Rumin, Y. Scaon, P. Schollhammer and J. Talarmin, *J. Chem. Soc., Dalton Trans.*, 1999, 2371–2383.

32 We chose to calibrate the peak currents using $[Fe_2Cp_2(CO)_2(\mu\text{-}SMe)_2]$ rather than ferrocene as a reference one-electron couple, making the reasonable assumption that $[Fe_2Cp_2(CO)_2(\mu\text{-}SMe)_2]$, $[Fe_2(CO)_6\{\mu\text{-}SCH_2XCH_2S\}]$ (**1**, **2**), and $[Fe_2(CO)_5L_{NHC}(\mu\text{-pdt})]$ (**3**) have similar diffusion coefficients. $D^{1/2}$ for ferrocene is about 1.6 times larger than for $[Fe_2Cp_2(CO)_2(\mu\text{-}SMe)_2]$.[33] This method was preferred to coulometry to determine the number of electrons involved in the reduction because of the existence of follow-up reactions that may be prominent on the longer time scale of bulk electrolyses; the following chemistry is thus susceptible to affect the coulometrically measured n value;[34] controlled-potential electrolysis of **1b** at −1.65 V led to extensive decomposition of the complex after the passage of *ca.* 2 F mol^{-1} **1b**.

33 T. Gennett, W. E. Geiger, B. Willett and F. C. Anson, *J. Electroanal. Chem. Interfacial Electrochem.*, 1987, **222**, 151–160.

34 D. T. Pierce and W. E. Geiger, *J. Am. Chem. Soc.*, 1992, **114**, 6063–6073, and references cited therein.

35 A. J. Downard, A. M. Bond, A. J. Clayton, L. R. Hanton and D. A. McMorran, *Inorg. Chem.*, 1996, **35**, 7684–7690.

36 (*a*) The peak to peak separation for the first reduction of **1** and **2** also increases with increasing v (Table 1), which is partly due to uncompensated solution resistance. The heterogeneous electron transfer rate constants k_s calculated from ΔE_p^{red2} following the procedure of Nicholson[36b] (k_s^{red2}(**1**) ∼6 × 10^{-4} cm s^{-1}; k_s^{red2}(**2**) ∼4 × 10^{-5} cm s^{-1}), were in reasonable agreement with those estimated (k_s^{red2}(**3a**) ∼8 × 10^{-4} cm s^{-1}; k_s^{red2}(**2**) ∼4 × 10^{-5} cm s^{-1}) by digital simulations of CV curves using DigiElch 2.0[37] with Cdl = 1.5 μF and Ru = 85 Ω; the diffusion coefficients for **3a** and **2** used in the calculations of k_s and in the simulations were worked out from the CV peak current i_p^{red1} at scan rates such that the first reduction of the complexes is a reversible one-electron transfer ($v \geq 10$ V s^{-1}). The diffusion coefficients of the anion and dianion were assumed to be identical to those of the neutral complexes **3a** and **2**; (*b*) R. S. Nicholson, *Anal. Chem.*, 1965, **37**, 1351.

37 For detailed information concerning DigiElch, see www.elchsoft.com and the following publications: (*a*) M. Rudolph, *J. Electroanal. Chem.*, 2003, **543**, 23–29; (*b*) M. Rudolph, *J. Electroanal. Chem.*, 2004, **571**, 289–307; (*c*) M. Rudolph, *J. Comput. Chem.*, 2005, **26**, 619–632; (*d*) M. Rudolph, *J. Comput. Chem.*, 2005, **26**, 633–641; (*e*) M. Rudolph, *J. Comput. Chem.*, 2005, **26**, 1193–1204.

38 M. D. Ryan, *J. Electrochem. Soc.*, 1978, **125**, 547–555.

39 F. Robin, R. Rumin, J. Talarmin, F. Y. Pétillon and K. W. Muir, *Organometallics*, 1993, **12**, 365–380.

40 For complex **2**, the reduction current measured at slow scan rate is also larger under CO than under Ar as shown in Fig. S2†.

41 (*a*) In the case of $[Fe_2(CO)_5(PTA)(\mu\text{-pdt})]$ (PTA = 1,3,5-triaza-7-phosphaadamantane, $P(CH_2)_6N_3$), a product peak that is suppressed in the presence of CO was attributed to the neutral MeCN-substituted derivative formed from the parent anion in an ETC process.[3e] In the present case, it is unlikely that product **P1** is $[Fe_2(CO)_5(CH_3CN)\{\mu\text{-}SCH_2XCH_2S\}]$. The ^{t}BuNC-substituted derivative electrogenerated from **1a** by replacement of one CO by a ^{t}BuNC ligand in an ETC process reduces at E_p^{red} = −1.83 V.[41b] From the reduction potentials of **1a** and of the ^{t}BuNC-substituted complex, and from the ligand parameter P_L[42] for MeCN (P_L = −0.58 V[42]), CO (P_L = 0 V[42]) and ^{t}BuNC (P_L = −0.44 V[43]), the reduction of $[Fe_2(CO)_5(CH_3CN)\{\mu\text{-}SCH_2N(R)CH_2S\}]$ is expected to occur around −1.9 V, a potential ∼0.2 V less negative than that of product **P1**. On the other hand, complex **3a** which derives from **2** by replacement of one carbonyl by a N-heterocyclic carbene ligand reduces at −2 V (see text), and it has been reported that $[Fe_2(CO)_5(CH_3CN)\{\mu\text{-}S(CH_2)_3S\}]$ undergoes an irreversible reduction at −1.68 V.[10a] Taken together, these results suggest that the reduction around −2.1 V is most probably due to an anionic species rather than to the neutral $[Fe_2(CO)_5(NCCH_3)\{\mu\text{-}SH_2XCH_2S\}]$. It is

therefore reasonable that product **P1** is the dianion with two bridged {Fe–Fe} units that was shown to form from $\mathbf{2}^{-}$,[4a,13b] and that was suggested[13b] as a reduction product of an analogue of **3a**. However, our DFT calculations suggest that this reaction will be hindered by the bulky R substituent of the N bridgehead atom in **3a**; (*b*) J.-F. Capon, F. Gloaguen, F. Y. Pétillon, P. Schollhammer and J. Talarmin, unpublished results.

42 J. Chatt, C. T. Khan, G. J. Leigh, C. J. Pickett and D. R. Stanley, *J. Chem. Soc., Dalton Trans.*, 1980, 2032–2038.

43 A. J. L. Pombeiro, C. J. Pickett and R. L. Richards, *J. Organomet. Chem.*, 1982, **224**, 285–294.

44 (*a*) For leading references, see W. E. Geiger, *Prog. Inorg. Chem.*, 1985, **33**, 275–352; (*b*) D. H. Evans and K. M. O'Connell, in *Electroanalytical Chemistry*, ed. A. J. Bard, M. Dekker, New York, 1986, vol. 14, pp. 113–207; (*c*) F. Y. Pétillon, P. Schollhammer and J. Talarmin, in *Encyclopedia of Electrochemistry*, ed. A. J. Bard and M. Stratman, Wiley-VCH, Weinheim, vol. 7, 2006, pp. 565–590, and references therein.

45 (*a*) B. Zhuang, J. W. McDonald, F. A. Schultz and W. E. Newton, *Organometallics*, 1984, **3**, 943–945; (*b*) B. Zhuang, J. W. McDonald, F. A. Schultz and W. E. Newton, *Inorg. Chim. Acta*, 1985, **99**, L29–L31; (*c*) D. A. Smith, B. Zhuang, W. E. Newton, J. W. McDonald and F. A. Schultz, *Inorg. Chem.*, 1987, **26**, 2524–2531; (*d*) J. B. Fernandes, L. Qun Zhang and F. A. Schultz, *J. Electroanal. Chem. Interfacial Electrochem.*, 1991, **297**, 145–161; (*e*) D. Uhrhammer and F. A. Schultz, *J. Phys. Chem. A*, 2002, **106**, 11630–11636.

46 (*a*) J. Courtot-Coupez, M. Guéguen, J. E. Guerchais, F. Y. Pétillon, J. Talarmin and R. Mercier, *J. Organomet. Chem.*, 1986, **312**, 81–95; (*b*) M. El Khalifa, F. Y. Pétillon, J.-Y. Saillard and J. Talarmin, *Inorg. Chem.*, 1989, **28**, 3849–3855.

47 J. P. Collman, R. K. Rothrock, R. G. Finke, E. J. Moore and F. Rose-Munch, *Inorg. Chem.*, 1982, **21**, 146–156.

48 J. Y. Cabon, C. Le Roy, K. W. Muir, F. Y. Pétillon, F. Quentel, P. Schollhammer and J. Talarmin, *Chem.–Eur. J.*, 2000, **6**, 3033–3042.

49 L. E. Bogan, Jr, D. A. Lesch and T. B. Rauchfuss, *J. Organomet. Chem.*, 1983, **250**, 429–438.

50 D. Seyferth, G. B. Womack and R. S. Henderson, *Organometallics*, 1986, **5**, 1568–1575.

51 Programs used: (*a*) G. M. Sheldrick, *SHELXL-97, Program for refinement of crystalstructures*, University of Göttingen, Germany, 1997; G. M. Sheldrick, *SHELXS-97, Program for solution of crystal structures*, University of Göttingen, Germany, 1997; (*b*) L. J. Farrugia, WINGX-A Windows Program for Crystal Structure Analysis, *J. Appl. Crystallogr.*, 1999, **32**, 837; (*c*) DENZO-SCALEPACKZ. Otwinowski and W. Minor, in *Methods in Enzymology Macromolecular Crystallography*, ed. C. W. Carter, Jr and R. M. Sweet, Academic Press, 1997, vol. 276 Part A, pp. 307–326.

52 M. J. Frisch, G. W. Trucks, H. B. Schlegel, G. E. Scuseria, M. A. Robb, J. R. Cheeseman, J. A. Montgomery, Jr., T. Vreven, K. N. Kudin, J. C. Burant, J. M. Millam, S. S. Iyengar, J. Tomasi, V. Barone, B. Mennucci, M. Cossi, G. Scalmani, N. Rega, G. A. Petersson, H. Nakatsuji, M. Hada, M. Ehara, K. Toyota, R. Fukuda, J. Hasegawa, M. Ishida, T. Nakajima, Y. Honda, O. Kitao, H. Nakai, M. Klene, X. Li, J. E. Knox, H. P. Hratchian, J. B. Cross, V. Bakken, C. Adamo, J. Jaramillo, R. Gomperts, R. E. Stratmann, O. Yazyev, A. J. Austin, R. Cammi, C. Pomelli, J. Ochterski, P. Y. Ayala, K. Morokuma, G. A. Voth, P. Salvador, J. J. Dannenberg, V. G. Zakrzewski, S. Dapprich, A. D. Daniels, M. C. Strain, O. Farkas, D. K. Malick, A. D. Rabuck, K. Raghavachari, J. B. Foresman, J. V. Ortiz, Q. Cui, A. G. Baboul, S. Clifford, J. Cioslowski, B. B. Stefanov, G. Liu, A. Liashenko, P. Piskorz, I. Komaromi, R. L. Martin, D. J. Fox, T. Keith, M. A. Al-Laham, C. Y. Peng, A. Nanayakkara, M. Challacombe, P. M. W. Gill, B. G. Johnson, W. Chen, M. W. Wong, C. Gonzalez and J. A. Pople, *GAUSSIAN 03 (Revision D.02)*, Gaussian, Inc., Wallingford, CT, 2004.

53 (*a*) A. D. Becke, *J. Chem. Phys.*, 1993, **98**, 5648–5652; (*b*) P. J. Stevens, J. E. Devlin, C. F. Chabalowski and M. J. Frisch, *J. Phys. Chem.*, 1994, **98**, 11623–11627; (*c*) C. Lee, W. Yang and R. G. Parr, *Phys. Rev. B*, 1988, **37**, 785–789.

54 M. Dolg, U. Wedig, H. Stoll and H. Preuss, *J. Chem. Phys.*, 1987, **86**, 866–872.

